Efficient tissue permittivity and conductivity mapping using standard MR images

Seung-Kyun Lee[1], Selaka Bandara Bulumulla[1], and Ileana Hancu[1]
[1]*GE Global Research, Niskayuna, NY, United States*

Target Audience: Researchers working on MR-based tissue electrical property mapping and novel image contrast

Introduction: In MR-based electrical property tomography [1-3], tissue electrical properties are calculated from the transmit RF field (B_1^+) map measured *in vivo* using the Helmholtz's equation (Eq. (1)). Whereas this equation is simple and popular, its practical utility has been limited in two regards: First, the phase of B_1^+ is not normally available from standard MR measurements, forcing one to make approximations which often lack rigorous theoretical background. Second, the SNR efficiency of B_1^+ amplitude mapping is typically inferior to standard MR imaging, causing a relatively long scan time in order to achieve acceptable SNR in the calculated electrical property values. In this work we present an alternative approach of tissue electrical property mapping based on standard MR images alone, without need for B_1^+ mapping. The method utilizes a rearranged wave equation which involves both the product and the ratio of B_1^+ and B_1^-. The product term is measurable in MRI with high SNR efficiency. Ignoring the ratio term allows expressing tissue conductivity and permittivity in terms of directly measureable quantities. The method was successfully applied to electrical property mapping in a phantom. We also obtained a preliminary measurement of conductivity in a volunteer's leg muscle.

Theory:

Equation: In a region of space where the tissue electrical properties are uniform, the Helmholtz equation can be applied to both the transmit and receive RF fields, Eqs. (1-2). Multiplying Eq. (1) with B_1^- and Eq. (2) with B_1^+, and adding them together, we obtain Eq. (3). Replacing $B_1^+B_1^-$ with $\left(\sqrt{B_1^+B_1^-}\right)^2$, we can re-write Eq. (3) as Eq. (4a,b). Ignoring the third term in Eq. (4a), and substituting $k^2 = \mu\epsilon_r\epsilon_0\omega^2 - i\mu\sigma\omega$ lead to Eqs. (5-6) that define the method of image-based tissue electrical property calculation.

(1)	$\nabla^2 B_1^+ + k^2 B_1^+ = 0$
(2)	$\nabla^2 B_1^- + k^2 B_1^- = 0$
(3)	$\nabla^2(B_1^+B_1^-) + 2k^2 B_1^+B_1^- - 2\nabla B_1^+ \cdot \nabla B_1^- = 0$
(4a)	$\frac{\nabla^2\sqrt{B_1^+B_1^-}}{\sqrt{B_1^+B_1^-}} + k^2 + k_{error}^2 = 0.$
(4b)	$k_{error}^2 \equiv \frac{1}{4}\nabla \ln\frac{B_1^-}{B_1^+} \cdot \nabla \ln\frac{B_1^-}{B_1^+}$
(5)	$\epsilon_r \approx -\frac{1}{\mu\epsilon_0\omega^2} Re\left(\frac{\nabla^2\sqrt{B_1^+B_1^-}}{\sqrt{B_1^+B_1^-}}\right)$
(6)	$\sigma \approx \frac{1}{\mu\omega} Im\left(\frac{\nabla^2\sqrt{B_1^+B_1^-}}{\sqrt{B_1^+B_1^-}}\right).$

Table 1. Equations used to derive and define the method.

Error estimation: One benefit of the method is that the approximation error is exactly known. In the limit where $B_1^+ = B_1^-$, the error term k_{error}^2 of Eq. (4) is zero. When the ratio B_1^-/B_1^+ is close to unity, the magnitude of k_{error}^2 can be estimated as $(1/4)k^2(B_1^-/B_1^+ - 1)^2$ by replacing $\nabla \rightarrow k$ and using $\ln(1+z) \approx z$ for small z. Here we have assumed that k represents the characteristic length scale of RF field variation in this region. Therefore, ignoring k_{error}^2 leads to an error in electrical property estimation by an amount that is quadratic to the fractional difference between B_1^+ and B_1^-. Finite-element RF simulation at 3 T shows that indeed $k_{error}^2 << k^2$ in human brain and breast for a transmit-receive birdcage coil.

Image-based tissue electrical property mapping: The amplitude and phase of $B_1^+B_1^-$ can be obtained from a small-angle gradient echo image and a spin-echo image, respectively. Therefore, Eqs. (5-6) allow mapping of electrical properties using standard MR images. Note that any image contrast that scales image intensity uniformly over a particular tissue type is cancelled in the fraction of Eqs. (5-6) and therefore does not affect ε_r and σ, except through errors in calculation of derivatives at the boundaries.

Methods: The above method was tested on a phantom consisting of three spheres; one filled with Wesson canola oil, and the other two filled with water with NaCl concentrations of 1.1 g/L and 2.2 g/L. Using a head birdcage coil, small-angle (α = 10°) gradient echo (GRE) and spin echo (SE) images were taken from seven, 3 mm-thick axial slices without a gap. In order to eliminate hardware-induced spurious phase from the SE images, the SE protocol was applied to a homogeneous silicone oil sphere and the resulting phase was subtracted. Laplacian calculation was performed using quadratic fitting [4]. For comparison, conventional B_1^+ map-based electrical property mapping was also performed on the same phantom following ref [3]. The total imaging time for the image-based and the B_1^+-based method was 5 and 10 minutes, respectively. An *in-vivo* scan of a volunteer's leg proceeded in a similar manner with a transmit-receive extremity coil. All measurements were done on a GE Discovery MR750 3.0T scanner.

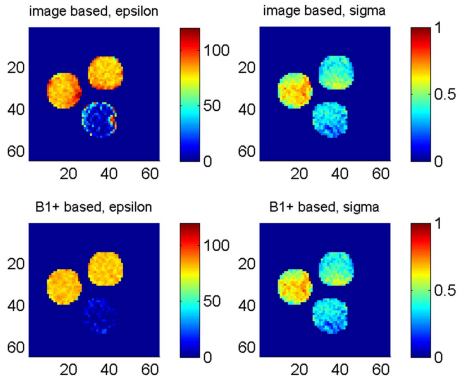

Figure 1. Relative permittivity and conductivity maps of an oil-water phantom from image-based (top row) and B_1^+-based methods (bottom).

Results: Figure 1 compares ε_r and σ calculated with the image- (top row), and B_1^+ - (bottom row) based methods. In each image, the bottom sphere is oil, and the top two spheres are water. The two methods produced similar conductivity and permittivity maps. Figure 2 shows the amplitude (up to a constant) and phase of $\sqrt{B_1^+B_1^-}$ (in radians), and calculated conductivity in an axial slice of a volunteer's leg.

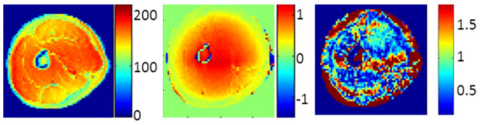

Figure 2. Amplitude of square root of GRE image (left), phase of square root of SE image (middle), and conductivity in [S/m] (right) of an axial slice of a leg.

Discussion: We have demonstrated a method to map electrical properties using standard MR images alone. The method does not require separation of transmit and receive RF field maps from an MR image, and has significant potential speed advantage compared to the B_1 map based methods. For *in-vivo* application, artifacts in Laplacian around the tissue contrast boundaries are a challenge. Effective tissue segmentation will be needed to ensure that calculation is done within a single tissue type avoiding boundary artifacts. More detailed comparison between the image- and B_1 map-based methods will be reported in a separate publication.

Acknowledgement: This work was supported in part by the NIH grant 1R01CA154433-01A1.

References: [1] Katscher U. et al, IEEE Trans Med Imaging 28:1365 (2009) [2] Bulumulla S. B. et al, ISMRM 2009, 3043 [3] Bulumulla S. B. et al, Concepts Magn Reson 41B:13 [4] Katscher U. et al, ISMRM 2012, 3482